Published online 18 August 2022

Nucleic Acids Research, 2022, Vol. 50, No. 16 ***9247–9259***
https://doi.org/10.1093/nar/gkac690

Regulation of nuclear DNA damage response by mitochondrial morphofunctional pathway

Nguyen Thi Kim Oanh[1,†], Ho-Soo Lee[1,†], Yong-Hyun Kim[1,2], Sunwoo Min[1], Yeon-Ji Park[1], June Heo[1,2], Yong-Yea Park[1], Won-Chung Lim[3,*] and Hyeseong Cho[1,*]

[1]Department of Biochemistry and Molecular Biology, Ajou University School of Medicine, Suwon, Republic of Korea, [2]Department of Biomedical Sciences, Graduate School of Ajou University, Suwon, Republic of Korea and [3]Department of Sports Medicine, College of Health Science, Cheongju University, Republic of Korea

Received June 23, 2022; Revised July 22, 2022; Editorial Decision July 23, 2022; Accepted August 03, 2022

ABSTRACT

Cells are constantly challenged by genotoxic stresses that can lead to genome instability. The integrity of the nuclear genome is preserved by the DNA damage response (DDR) and repair. Additionally, these stresses can induce mitochondria to transiently hyperfuse; however, it remains unclear whether canonical DDR is linked to these mitochondrial morphological changes. Here, we report that the abolition of mitochondrial fusion causes a substantial defect in the ATM-mediated DDR signaling. This deficiency is overcome by the restoration of mitochondria fusion. In cells with fragmented mitochondria, genotoxic stress-induced activation of JNK and its translocation to DNA lesion are lost. Importantly, the mitochondrial fusion machinery of MFN1/MFN2 associates with Sab (SH3BP5) and JNK, and these interactions are indispensable for the Sab-mediated activation of JNK and the ATM-mediated DDR signaling. Accordingly, the formation of BRCA1 and 53BP1 foci, as well as homology and end-joining repair are impaired in cells with fragmented mitochondria. Together, these data show that mitochondrial fusion-dependent JNK signaling is essential for the DDR, providing vital insight into the integration of nuclear and cytoplasmic stress signals.

INTRODUCTION

Cells are continuously exposed to endogenous and exogenous DNA damaging sources and an elegant nuclear machinery against DNA attack protects the genome by operating the DNA damage response (DDR) and repair pathways (1,2). In eukaryotes, an additional genome is present in the mitochondria, and communication between the nucleus and mitochondria is essential for the maintenance of genome integrity and cellular homeostasis. In response to nuclear DNA double-strand breaks (DSBs), ATM kinase is recruited to DSB sites via the sensor of MRE11/RAD50/NBS1 (MRN) complex (3,4). The activated ATM kinase phosphorylates a histone H2A variant, H2AX, at Ser139 to yield γH2AX, which triggers recruitment of MDC1. The interplay among these proteins cooperates to propagate γH2AX at DSB sites and to recruit downstream DDR factors (5). DDR signaling requires fine spatiotemporal regulation, which is achieved by specific histone posttranslational modifications such as ubiquitination and methylation (6,7) that can be recognized by 53BP1 and BRCA1 (8,9). In addition, ATM activates DNA damage checkpoint proteins of Chk1 and Chk2, which regulate cell cycle progression (10). Depending on the status of the cell-cycle phase, 53BP1-RIF1 and BRCA1 drive two major DSB repair pathways; non-homologous end joining (NHEJ) and homologous recombination (HR) (11,12).

In response to various stresses, mitochondria morphology can change rapidly. Mitochondria are highly motile organelles, and the dynamic properties of mitochondrial tubular networks are balanced by the flux of fusion and fission events. Mitochondrial fission is driven by cytosolic dynamin-related protein 1 (DRP1), which is recruited to the mitochondrial surface by proteins such as MFF, Fis1 and MIEF1/2 (MiD51/49) anchored to the outer mitochondrial membrane (OMM) (13–16). Three further dynamin-related GTPases control mitochondrial fusion: the mitofusins (MFN1 and MFN2) located within the OMM and optic atrophy 1 (OPA1) located within the inner mitochondrial membrane (IMM) (17,18). These mitochondria-shaping proteins drive morphological transition following cellular stresses. A number of stress stimuli including UV irradiation, nutrient deprivation, and the inhibition of protein synthesis can trigger transient mitochondrial hyperfu-

*To whom correspondence should be addressed. Tel: +82 312195052; Fax: +82 312195059; Email: hscho@ajou.ac.kr
Correspondence may also be addressed to Won-Chung Lim. Email: wonchlim@gmail.com
†The authors wish it to be known that, in their opinion, the first two authors should be regarded as Joint First Authors.
Present address: Nguyen Thi Kim Oanh, Department of Neurology, Mayo Clinic, 200 First St. SW, Rochester, MN 55905, USA.

sion (19,20). This stress-induced mitochondrial hyperfusion (SIMH) is orchestrated by MFN1 and OPA1 together with the IMM protein SLP2 (21). In general, SIMH mitigates cellular stress (22,23) and is considered as a prosurvival response. However, prolonged mitochondrial hyperfusion can increase production of reactive oxygen species (ROS), leading to aneuploidy and cellular senescence (24,25). Meanwhile, stimuli that alter mitochondrial function can result in fission of the organelle. In pancreatic beta cells, high glucose concentrations can induce mitochondrial fragmentation (26,27), and excessive mitochondrial fission appears to be a prerequisite for the induction of apoptosis (28). Meanwhile, accelerated mitochondrial division in cardiomyocytes in response to sustained hypertension can compensate for increased energy demand via mitophagy (29). Mitophagy can remove defective mitochondria, preventing the accumulation of dysfunctional mitochondria (30), and contributing to cellular homeostasis. Thus, transient and rapid mitochondrial morphological adaptation plays an important role in the response to cellular stress, which is important for cell adaptation and the determination of cell fate.

In addition to morphological transition, mitochondria respond to stress by signaling to the nucleus, which mainly contributes to the restoration of cellular homeostasis. Among various retrograde signals, the response to cytoplasmic mitochondrial DNA (mDNA) has been well documented, as it contributes to the induction of genes responsible for nuclear DNA (nDNA) damage response and repair. Mitochondria contain fewer DNA repair systems than nucleus (31) and mDNA is rapidly degraded, especially following mitochondrial DNA strand breaks (mtDSBs) (32,33). Intriguingly, mDNA in *Tfam*$^{+/-}$ cells is released into the cytoplasm and activates the cGAS-STING immune signaling pathway (34), while interferon-stimulated genes (ISGs) including ISG15, DTX3L and PARP family members (PARP9, 12 and 14) enhance the nDNA damage response and HR repair (35–37). In addition, cytoplasmic mitochondrial RNAs in cells with mtDSBs also stimulates expression of ISGs through the RIG-I-MAVS signaling pathway. Thus, it appears that nucleus and mitochondria tightly cooperate to deal with genomic damages to maintain cellular homeostasis. However, canonical DDR signaling may not directly recognize mtDSBs because p-ATM and γH2AX levels are not altered in cells with mtDSBs generated by mitochondria-targeted TALEN system (38).

In the present study, we examined whether canonical DDR is linked to mitochondrial morphological changes. We show that the mitochondria morphofunctional pathway closely interacts with the nuclear DDR, and cells deficient for mitochondrial fusion exhibit a substantial defect in nuclear DDR signaling. Intriguingly, we find that the MFN1/MFN2 mitochondrial fusion machinery establishes a signaling platform with Sab and the cytoplasmic stress kinase JNK on the mitochondria, and this platform is indispensable for JNK activation and subsequent ATM-mediated DNA repair. We conclude that the nuclear DDR integrates with cytoplasmic stress signals through the mitochondrial morphofunctional pathway following genotoxic stress.

MATERIALS AND METHODS

Reagents

Detailed information about antibodies used in this study is listed in Supplementary Table S2.

Biological resources

Human HEK293T, U2OS and EKSV cells and mouse embryonic fibroblasts (MEFs) were cultured in Dulbecco's modified Eagle's medium (DMEM, WELGENE) with high glucose. A549 cells were cultivated in RPMI and HeLa cells were cultured in DMEM. All media were supplemented with 10% heat-inactivated fetal bovine serum (FBS, Gibco BRL, Invitrogen) and 1% penicillin-streptomycin. U2OS-2-6-5 cell line as well as the U2OS cell lines stably expressing DR-GFP or EJ-GFP constructs were maintained in the same medium condition with additional puromycin (1 μg/ml). U2OS-2-6-5 cells harbor a mCherry-LacI-Fok1 nuclease fused to a destabilization domain (DD) and a modified estradiol receptor. Addition of Shield1 ligand and 4-hydroxytamoxifen (4-OHT) induces Fok1 nuclease expression in these cells, generating single DSB. U2OS cell lines stably expressing DR-GFP or EJ-GFP constructs were used to analyze HR or NHEJ repair, respectively. All cells were incubated in 5% CO_2 at 37°C.

Establishment of cells expressing shRNA

Silencing of endogenous MFN1 was carried out using short hairpin (sh)-activated gene silencing. Plasmids expressing shRNAs were constructed by synthesizing and annealing two cDNA oligonucleotides bearing the target sequences, a HindIII linker and a U6 terminator, which were ligated into BseRI and BamHI sites of pSHAG-1 (Cold Spring Harbor Laboratory, Cold Spring, NY). Then, the DNA region encoding the U6 promoter and shRNA in pSHAG-1 was subcloned into NotI and BamHI sites of pREP4 (Invitrogen, Carlsbad, CA). Twenty-four hours after transfection with pREP4 vector, cells were grown in DMEM containing 300 μg/ml of hygromycin B for 2–3 weeks. Hygromycin-resistant clones were obtained and maintained in DMEM containing 50 μg/ml of hygromycin B for the experiment.

RNA interference and plasmid transfection

Human-specific siRNAs for MFN1, SAB and JNK were synthesized by Bioneer (Supplementary Table S1). U2OS and A549 cells were transfected with 100 nM of siRNAs using Lipofectamine™2000 (Invitrogen), according to the manufacturer's instructions and harvested 48 h post-transfection. Plasmid transfections were performed using polyethylenimine (PEI, Polysciences) and cells harvested 48 hr post-transfection.

Immunoprecipitation and immunoblot analysis

For immunoprecipitation, cells were lysed with RIPA buffer (50 mM Tris–HCl [pH7.4], 150 mM NaCl, 1% NP-40, 0.1% SDS, 0.1% sodium deoxycholate, 5 mM EDTA and 5 mM EGTA) supplemented with protease and phosphatase

inhibitors and the resulting whole-cell lysates incubated with 1 μg of the indicated antibodies at 4°C for 10–12 h with agitation. After further incubation with protein A-sepharose beads (GE Healthcare Bio-Science AB) for 1 h 30 min, the bead-bound immunoprecipitants were washed with RIPA buffer four times and eluted in 2× SDS sample buffer by boiling for 5 min. For immunoblot analysis, cells were lysed in RIPA buffer and the resulting whole-cell extracts resolved by SDS-PAGE. Proteins were transferred onto nitrocellulose membrane (Millipore) and immunoblots were visualized using ECL (Bio-Rad).

Immunofluorescence microscopy

U2OS, MEF and HeLa cells were seeded onto coverslips in six-well plates. To visualize mitochondria, cells were stained with 125 nM of Mitotracker Red™ (Molecular Probes) for 30 min before harvest. Cells were fixed with 4% paraformaldehyde in phosphate-buffered saline (PBS) for 10 min at room temperature. Fixed cells were permeabilized with methanol for 20 min at –20°C. For immunofluorescent staining, cells were blocked with 5% bovine serum albumin in PBS for 1 h at room temperature, followed by primary antibody incubation overnight at 4°C. Cells were washed three times and incubated with a fluorescence-conjugated secondary antibody for 1 h at room temperature. For image acquisition, Nikon A1R-A1 Confocal Microscope system with 60× 1.4 NA Plan-Apochromat objective (Nikon Instrument Inc.) or LSM710 with 63× 1.4 NA Plan-Apochromat objective (Carl Zeiss) were used at the Three-dimensional immune system imaging core facility of Ajou University. Images were analyzed by the NIS elements C program or the ZEN 2011 program and Image processing and quantification were carried out with ImageJ.

DNA double-strand break repair assays

DR-GFP or EJ-GFP containing stable cell lines and the I-Sce1 constructs were kindly provided by Dr Jeremy Stark (City of Hope National Medical Center). DR-GFP 293T cells are developed to measure HR-mediated DSB repair efficiency. DR-GFP contains a modified GFP gene containing an I-Sce1 site and in-frame termination codons, and a nonfunctional internal GFP fragment (iGFP), which can be used as a template for HR resulting in a production of functional GFP gene (39). EJ-GFP cells are used to measure NHEJ-mediated DSB repair. EJ5-GFP contains a promoter that is separated from a GFP coding cassette by a puromycin gene flanked by two I-Sce1 sites in the same orientation. Once the puromycin gene is excised by I-Sce1-induced DSBs, NHEJ can lead to the joining of the promoter to the GFP expression cassette, resulting in the restoration of the GFP+ gene (40). DR-GFP or EJ-GFP expressing cells were transfected with the indicated siRNAs or a control (shLuc). Twenty-four hours post-transfection, cells were further transfected with 10 μg of the pCBA-I-Sce1 plasmid. Forty-eight hours post-transfection, cells were collected and analyzed by flow cytometry. The frequency of GFP+ cells was determined by FACS Canto II cytometer.

Alkaline comet assay

Cells were treated with 500 μM of H_2O_2 for 30 min (R0) and released after 4 h (R4), and Alkaline Comet Assay was performed using reagents from Trevigen in accordance with the manufacturer's protocol. Imaging was performed with a fluorescence microscope and Tail Moment determined using the OpenComet analysis software. Fifty or more comets were analyzed for each experiment.

Mitochondrial fragmentation count (MCF)

Cells were stained with Mitotracker Red™ and imaged with confocal microscopy to assess the mitochondrial network structure. The acquired images were background subtracted, filtered (median), thresholded, and binarized to identify mitochondrial segments, using NIS Elements AR microscope imaging software. Continuous mitochondrial structures were counted with the particle counting subroutine and normalized to the total mitochondrial area (in pixels) for each cell imaged.

- Mitochondrial fragmentation count (MCF): number of particles × 10 000/total mitochondrial pixels.

Statistical analysis

All values in this study are reported as mean ± SEM. The average of at least three independent experiments is shown. Two-sided unpaired Student's t test was used to assess statistical significance. In all figures, $*P < 0.05$, $**P < 0.005$ and $***P < 0.001$ versus the control.

RESULTS

DNA damage response signaling is sensitive to mitochondrial morphodynamics

Cells respond promptly to deleterious genotoxic stresses, preserving the nuclear genome through the DDR (1,10). Mitochondria also respond to cellular stresses; in particular, mitochondrial fusion can mitigate stress (20–23). However, it remains elusive whether the canonical DDR is linked to morphodynamic changes of mitochondria. To assess the connection between the DDR and mitochondrial dynamics, we disrupted mitochondrial fusion and examined the DDR signaling after treatment with the radiomimetic agent, phleomycin (Phleo). First, we examined whether mitochondria undergo transient mitochondrial hyperfusion against DNA damage. We traced the mitochondrial morphological changes by measuring mitochondria fragmentation count (MFC), which determines acquired image of mitochondria segment among total mitochondria area under a time-lapse microscopy (41). Relatively mild DNA damage was used to prevent mitochondrial damage or fragmentation, leading to ROS generation and secondary nuclear DNA damage (42). Following treatment with 100 μg/ml of Phleo, MFC was reduced in 1 hr and further dropped in 2 h (Supplementary Figure S1A), suggesting that mitochondria hyperfuse against DNA damage stress. Likewise, when U2OS cells were treated with 500 μM of H_2O_2, mitochondrial hyperfusion was observed in 30–60 min after treat-

ment. This hyperfusion was resolved within 2 h (Supplementary Figure S1B). Thus, all our experiments were set up within 2 h. Next, mitochondria fusion was disrupted by decreasing MFN1 expression using shRNA and assessed the DDR signaling by monitoring the γH2AX level, a molecular marker for DSBs. A dose-dependent increase in γH2AX was observed in U2OS cells following Phleo treatment for 2 h; however, this was disrupted by MFN1 shRNA treatment (Figure 1A). Quantification of immunoblots displayed a significant reduction of γH2AX levels in MFN1 knockdown (KD) cells after treatment with 50 or 100 ug/ml of Phleo (Figure 1A, right panel). In these cells, mitochondria fragmentation was significantly increased by MFN1 depletion (Figure 1B, Supplementary Figure S2A). Similarly, a significant reduction of γH2AX levels was also observed in cells treated with OPA1 shRNA along with increase of mitochondrial fragmentation (Figure 1C, D). A recent report by Yu *et al.* revealed that human Fis1 (hFis1) impairs pro-fusion activity by blocking the GTPase activity of mitofusins and OPA1 (43). When cells overexpressing hFis1 were exposed to Phleo, a considerable reduction in γH2AX and elevation in MFC were observed (Figure 1E, F). Next, we overexpress the FLAG-tagged MFN in MFN1 knockdown (KD) and examined whether restoration of mitochondria fusion activity would restore the DDR signaling. As expected, the substantial reduction in γH2AX observed in MFN1 KD cells was reversed by the introduction of FLAG-MFN1 (Figure 1G), and mitochondrial elongation was restored (Supplementary Figure S2B). In addition, we also observed that cells treated with other DNA damaging agents including H_2O_2 and the DNA alkylating agent, MMS showed reduced γH2AX levels in MFN1 knockout (KO) cells (Supplementary Figure S2C, D). Together, these findings revealed that canonical DDR signaling on the chromatin is tightly linked to mitochondria morphodynamics.

The mitochondrial network undergoes fragmentation in sustained high-glucose conditions through accelerated fission (26,27). Morphological homeostasis of mitochondria is especially important in patients with hyperglycemia or type 2 diabetes (44,45). Time-lapse fluorescence microscopy revealed that in the presence of 50 mM of glucose, fragmentation occurred after 5–6 h (Supplementary Figure S3A). Therefore, we investigated whether DDR signaling is altered in cells exposed to high-glucose conditions. U2OS cells were cultivated in the media with additional glucose (25, 50 mM) for 5 h before Phleo was added for an additional 1 h. The accumulation of γH2AX foci and protein decreased significantly in the presence of high glucose, while MFC increased (Figure 1H, Supplementary Figure S3B). Release from high-glucose stress into normal media led to a recovery in γH2AX levels within 8 h (Figure 1I, Supplementary Figure S3C). Together, these data indicate that the DDR signaling on the chromatin relies on the maintenance of mitochondrial fusion.

JNK activation under genotoxic stress is impaired in cells harboring fragmented mitochondria

Cells activate several cytosolic kinases in response to genotoxic stress (46,47). To examine whether these kinases influence mitochondrial dynamics, we sought to identify cytosolic stress-induced kinases with altered activity upon treatment with MFN1 shRNA. Phleo-induced phosphorylation of c-JUN-N-terminal kinase (JNK) and mTOR was attenuated in MFN1 depleted cells, while the phosphorylation of Akt, AMPK, p70, and ERK1/2 remained unchanged or was elevated (Figure 2A). The siRNA-mediated knockdown of MFN1 in U2OS cells consistently decreased the accumulation of JNK phosphorylation, accompanied by loss of γH2AX accumulation (Figure 2B). Inversely, introduction of FLAG-MFN1 into MFN1 KD cells restored JNK activity upon treatment with H_2O_2 (Figure 2C). Overexpression of hFis1 and silencing of OPA1 suppressed H_2O_2-induced phosphorylation of JNK (Figure 2D, E). Similarly, hyperglycemia-induced mitochondria fragmentation significantly decreased the accumulation of p-JNK, resulting in inefficient γH2AX accumulation (Figure 2F). Active JNK translocates from the cytoplasm to the nucleus, where it phosphorylates target proteins (48). Therefore, we next sought to determine whether nuclear accumulation of phosphorylated JNK was defective in cells deficient for mitochondrial fusion. To this end, we utilized *AsiS1* cells in which the Fok1 endonuclease makes a single DSB site upon tamoxifen treatment (49). These cells were treated with H_2O_2 to activate cytoplasmic JNK and examined the accumulation of p-JNK at the DSB site by immunofluorescence staining. Interestingly, nuclear accumulation of p-JNK was dramatically reduced in MFN1 knockdown cells (Figure 2G), and the p-JNK foci at the DSB site were almost completely lost in these cells (Figure 2G, right panel). Together, these data indicate that mitochondrial fusion is a critical for JNK activation and subsequent DDR signaling.

Deficiency in mitochondrial fusion disrupts the ATM-mediated DNA damage response

Because both γH2AX accumulation and the p-JNK levels were reduced in cells with deficient in mitochondrial fusion, we investigated whether the DDR including γH2AX accumulation is regulated by JNK activity. In response to DNA damage, ATM kinase phosphorylates H2AX at Ser139, generating γH2AX that propagates for mega-bases around DNA lesions (5). In turn, γH2AX creates a platform for propagating DDR signaling cascades by recruiting mediator of DNA damage checkpoint protein 1 (MDC1), breast cancer susceptibility 1 (BRCA1) and p53-binding protein 1 (53BP1) along with the damage repair machinery (8,9). In the non-canonical pathway, it has been shown that activated JNK under severe DNA damage can directly phosphorylate H2AX, triggering DNA fragmentation (50). When we co-treated cells with Phleo and two concentrations (25 or 50 μM) of the JNK inhibitor SP600125, γH2AX levels were suppressed in a dose-dependent manner (Figure 3A). This observation was confirmed by immunofluorescence staining showing that formation of γH2AX foci was significantly reduced by SP600125 treatment (Supplementary Figure S4A). In addition, we noted that not only γH2AX but also p-ATM levels were reduced by co-treatment with the JNK inhibitor (Figure 3A, Supplementary Figure S4B) both in U2O2 and human lung adenocarcinoma EKVX cells (Supplementary Figure S4C). Indeed,

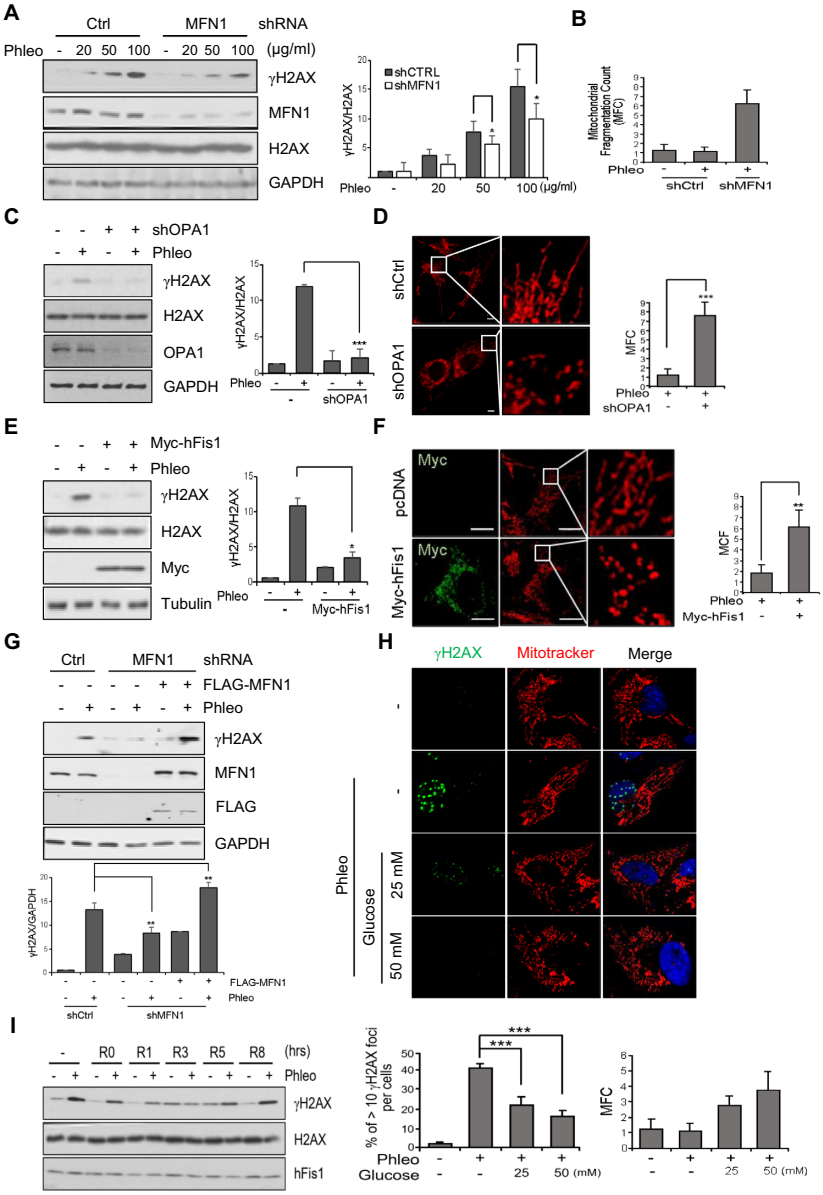

Figure 1. Deficient mitochondria fusion mitigates the DNA damage response signaling. (**A**) MFN1 stably depleted U2OS cells were treated with increasing concentrations of phleomycin (Phleo), a DSB-mimetic reagent for 2 h. The cells were lysed and immunoblotted with the indicated antibodies and quantification was shown as fold change relative to the control. Bars represent mean ± SEM from three independent experiments; * $P < 0.05$ versus control by two-sided unpaired Student's t-test. (**B**) Mitochondrial morphology visualized by Mito-Tracker (Supplementary Figure S2A) was quantified by mitochondrial fragmentation count (MFC). Bars represent mean ± SEM from three independent experiments; $n_{shCtrl} = 32$, $n_{shMFN1} = 22$ cells. ** $P < 0.005$ versus control siRNA by two-sided unpaired Student's *t*-test. (**C**) U2OS cells transfected with OPA1 shRNA were treated with Phleo for 2 h and subjected to immunoblotting with the indicated antibodies. Band intensities of the γH2AX levels in immunoblot were measured by using imageJ. Bars represent mean ± SEM from three independent experiments. *** $P < 0.001$ versus control shRNA by two-sided unpaired Student's *t*-test. (**D**) U2OS cells transfected with OPA1 shRNA were treated with Phleo for 2 h and immunostained with MitoTracker (red). Bars represent mean ± SEM from three independent experiments; $n_{shCtrl} = 25$, $n_{shOPA1} = 28$ cells. *** $P < 0.001$ versus control shRNA by two-sided unpaired Student's *t*-test. Scale bar, 10 μm. (**E**) Myc-hFis1 plasmid was transfected into U2OS cells and treated with Phleo for 2 h. Cell lysates were subjected to immunoblot analysis with indicated antibodies. Bars represent mean ± SEM from three independent experiments. *** $P < 0.001$ versus control shRNA by two-sided unpaired Student's *t*-test. (**F**) Myc-hFis1 plasmid was transfected into U2OS cells and treated with Phleo for 2 h. Cells were subjected to immunofluorescence stained with anti-Myc (green) antibody and Mitotracker (red). Mitochondrial morphological change was quantified by determination of MFC. Bars represent mean ± SEM from three independent experiments; $n_{pcDNA} = 30$, $n_{Myc\text{-}hFis1} = 28$ cells. *** $P < 0.001$ versus control by two-sided unpaired Student's *t*-test. Scale bar, 10 μm. (**G**) MFN1 depleted U2OS cells reconstituted with Flag-MFN1 were treated with Phleo for 2 h, and subjected to immunoblotting. Bars represent mean ± SEM from three independent experiments. *** $P < 0.001$ versus control shRNA by two-sided unpaired Student's *t*-test. (**H**) U2OS cells were exposed to 25, 50 mM of glucose for 5 h before treatment with Phleo for additional 2 h. Cells were stained with MitoTracker (red) followed by immunostaining with anti-γH2AX (green) antibody and DAPI (blue). Lower panel (left) show the percentage of cells containing >10 γH2AX foci per cell (left) in three independent experiments; $n_{non} = 278$, $n_{glu\ 25} = 310$, $n_{glu\ 50} = 286$. Lower right panel shows the MFC value. Bars represent mean ± SEM from three independent experiments; $n_{non} = 32$, $n_{glu\ 25} = 17$, $n_{glu\ 50} = 21$ cells. *** $P < 0.001$ versus control by two-sided unpaired Student's *t*-test. Scale bar, 10 μm. (**I**) U2OS cells were subjected to the 50 mM of glucose treatment for 5 h and released to fresh medium. The cells were pre-treated with Phleo for 2 h before harvest as indicated times and immunoblotted with the indicated antibodies.

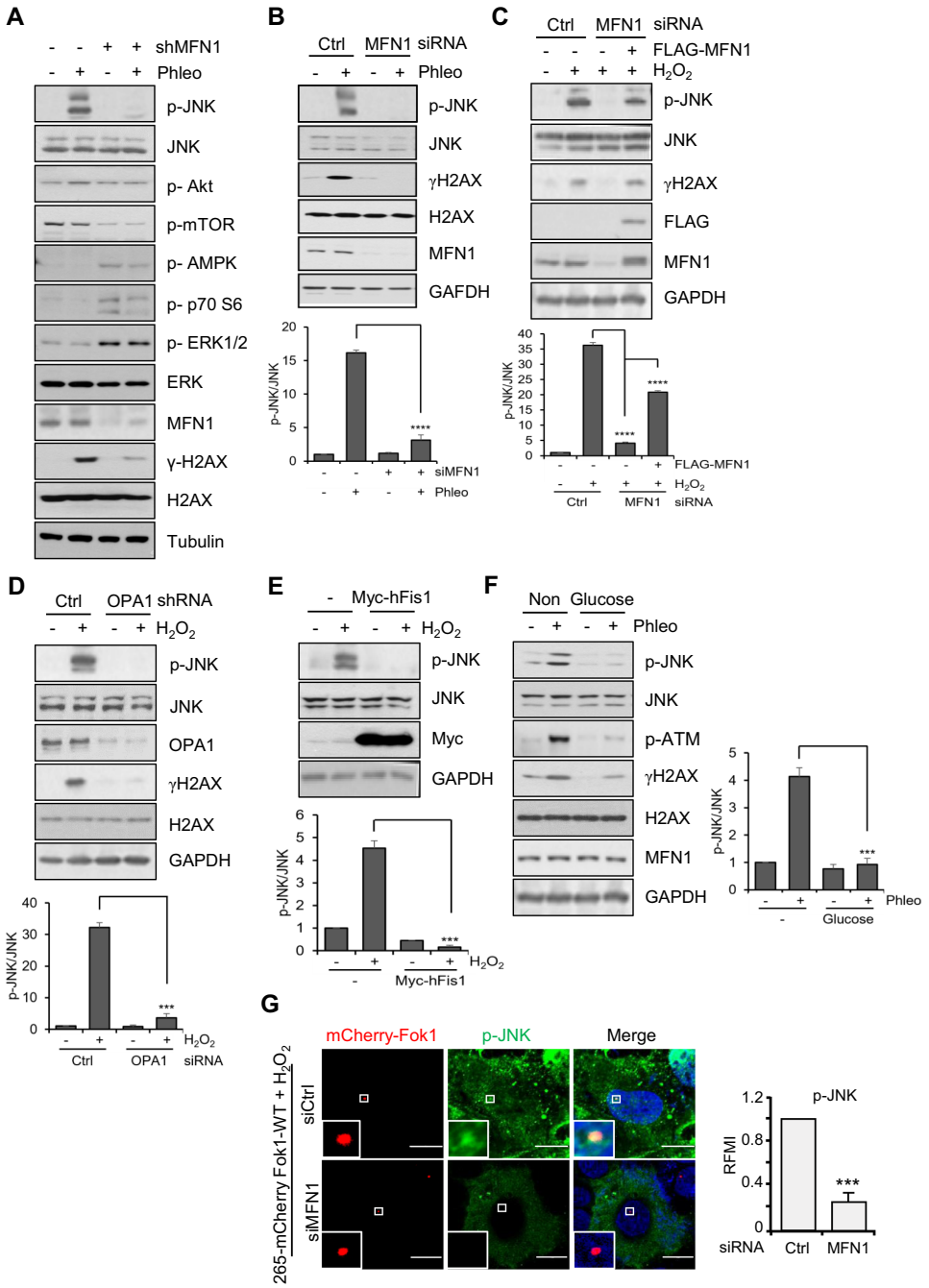

Figure 2. JNK activation under genotoxic stress is impaired in cells with fusion-deficient mitochondria. (**A**) U2OS control cells and MFN1 shRNA cells were treated with Phleo for 2 h and subjected to immunoblotting with indicated antibodies. (**B**) U2OS cells transfected with control or MFN1 siRNA were treated with Phleo for 2 h and subjected to immunoblotting with indicated antibodies. Quantification on the phospho-JNK levels was shown at the lower panel. Bars represent mean ± SEM from three independent experiments. *** $P < 0.001$ versus control siRNA by two-sided unpaired Student's *t*-test. (**C**) Flag-MFN1 plasmid was transfected into MFN1 depleted cells and treated with H_2O_2 for 20 min, and cells were immunoblotted. Band intensities of p-JNK level were determined by ImageJ. Bars represent mean ± SEM from three independent experiments. *** $P < 0.001$ versus control shRNA by two-sided unpaired Student's *t*-test. (**D**) U2OS cells were transfected with OPA1-targeting shRNA for 48 h and treated with H_2O_2 for 20 min. The cell lysates were processed for immunoblotting analysis using indicated antibodies and quantification of p-JNK level was determined by using ImageJ. Bars represent mean ± SEM from three independent experiments. *** $P < 0.001$ versus control shRNA by two-sided unpaired Student's *t*-test. (**E**) Myc-hFis1 plasmid was transfected into U2OS cells and cells were obtained with H_2O_2 treatment for 20 min. The lysates were immunoblotted with indicated antibodies and expression levels of the phospho-JNK were quantified from western blot images. Bars represent mean ± SEM from three independent experiments. *** $P < 0.001$ versus control shRNA by two-sided unpaired Student's *t*-test. (**F**) U2OS cells were treated with 50 mM of glucose for 5 hr and subjected to Phleo for additional 2 hr before harvest, followed by immunoblotted with indicated antibodies. Quantification of p-JNK band intensities was measured using imageJ. Bars represent mean ± SEM from three independent experiments. *** $P < 0.001$ versus control shRNA by two-sided unpaired Student's t-test. (**G**) U2OS 2–6-5 cells were transfected with siRNA for MFN1 and DSB was induced by addition of 4-OHT and shield1 for 4 h. The cells were then treated with H_2O_2 for 20 min before harvest. The intensity of p-JNK level at DSB foci was shown as relative fluorescence mean intensity (RFMI). Bars represent mean ± SEM from three independent experiments; $n_{siCtrl} = 36$, $n_{siMFN1} = 42$ cells. *** $P < 0.001$ by Student's *t*-test. scale bars, 10 μm.

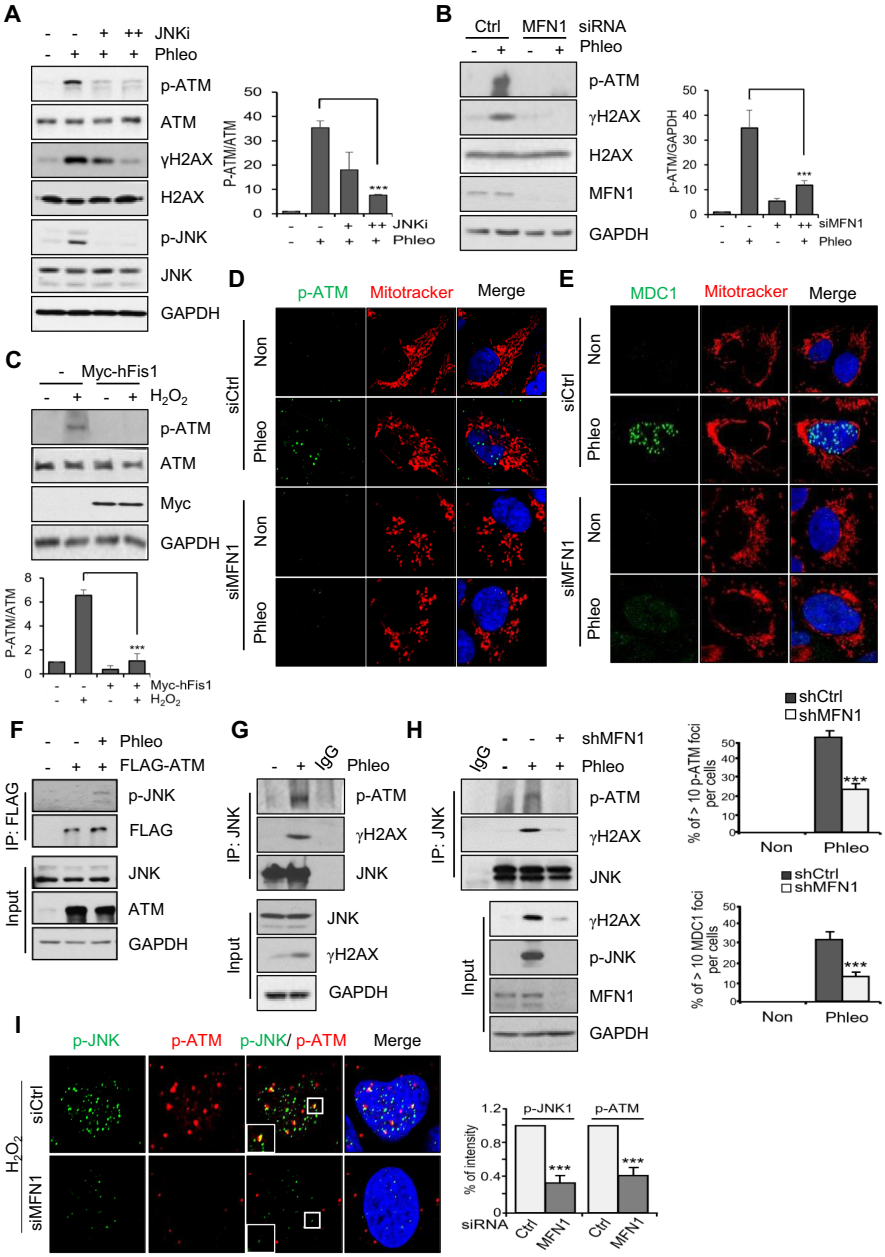

Figure 3. Mitochondrial fusion modulates ATM-dependent DNA damage response signaling. (**A**) U2OS cells were treated with a JNK inhibitor (SP600125, 25 μM or 50 μM) in the presence of Phleo for 2 h, followed by immunoblotting with the indicated antibodies. The p-ATM level was quantified by using imageJ. Bars represent mean ± SEM from three independent experiments. *** $P < 0.001$ versus control shRNA by two-sided unpaired Student's *t*-test. (**B**) U2OS cells were transfected with control or MFN1 siRNA and harvested after treatment with Phleo for 2 h. Cells were immunoblotted with indicated antibodies and the phospho-ATM levels were quantified from western blot images. Bars represent mean ± SEM from three independent experiments. *** $P < 0.001$ versus control shRNA by two-sided unpaired Student's *t*-test. (**C**) U2OS cells were transfected with Myc-hFis1 and treated with H_2O_2 for 20 min. Cells were immunoblotted with indicated antibodies. Expression levels of the p-ATM were measured from western blot images. Bars represent mean ± SEM from three independent experiments. *** $P < 0.001$ versus control shRNA by two-sided unpaired Student's *t*-test. (**D**) Cells stably expressing the MFN1 shRNA were treated with Phleo for 2 hr and subjected to immunostaining. Images were obtained from representative cells: p-ATM (green), MitoTracker (red) and 4,6-diamidino-2-phenylindole (DAPI; blue). Cells were counted in three independent experiments; $n_{shCtrl} = 242$, $n_{shMFN1} = 289$ cells. scale bars, 10 μm. (**E**) MFN1-depleted U2OS cells were treated with Phleo for 2 h and subjected to immunostaining. Cells were analysed by immunofluorescence staining: MDC1 (green), MitoTracker (red) or DAPI (blue). Lower panels show the percentage of cells with >10 p-ATM foci per cell, or cells of >10 MDC1 foci per cell in three independent experiments; $n_{shCtrl} = 262$, $n_{shMFN1} = 324$ cells. scale bars, 10 μm. (**F**) U2OS cells transfected with FLAG-ATM vector and harvested after treatment with Phleo for 2 h. Cells were immunoprecipitated with anti-FLAG antibodies and immunobltted with the p-JNK antibodies. (**G**) Endogenous JNK were immunoprecipitated with anti-JNK antibody, followed by immunoblotting with p-ATM antibodies. (**H**) Cells stably expressing MFN1 shRNA were treated with Phleo for 2 h. The cell lysates were immunoprecipitated with anti-JNK antibody and immunoblotted with anti-p-ATM antibodies. (**I**) U2OS cells stably expressing the MFN1 shRNA were treated with H_2O_2 for 20 min, followed by immunofluorescence staining with anti-p-JNK (green), p-ATM (red) and DAPI (blue). The graphs represent mean ± SEM from three independent experiments showing relative signal intensity of p-JNK or p-ATM (siCtrl $n = 33$ and siMFN1 $n = 35$) at the nucleus. *** $P < 0.001$ versus control siRNA by two-sided unpaired Student's *t*-test.

p-ATM levels were reduced in MFN1-depleted cells (Figure 3B) and hFis1-overexpressing cells (Figure 3C) under genotoxic stress. Likewise, the foci formation of p-ATM and MDC1 was significantly reduced in MFN1 KD cells (Figure 3D, E). Quantification on foci formation with 10 or more foci per cells showed a significant difference between control and MFN1 KD cells (Figure 3D, E bottom panels). Thus, it appeared that failure in the DDR signaling in cells defective in mitochondria fusion is a consequence of low JNK activity in these cells.

Next, we investigated the mechanism by which JNK regulates ATM activation. The physical interaction between ATM and JNK was examined by immunoprecipitation in 293T cells transfected with FLAG-tagged ATM 48 hr prior to DNA damage. We found that FLAG-tagged ATM interacts with activated p-JNK under DNA damaging condition (Figure 3F). Similar results were obtained at endogenous levels showing that JNK binds efficiently to p-ATM and γH2AX upon DNA damage (Figure 3G). On the other hand, the interaction between p-ATM and JNK was severely damaged in MFN1 KD cells (Figure 3H). Together, these data indicate that mitochondrial fusion is a critical for JNK activation and subsequent DDR signaling (Figure 3I). Together, these data show that mitochondrial fusion–mediated activation of JNK is an essential modulator of ATM-dependent DDR signaling.

The mitochondrial fusion machinery interacts with Sab and JNK under genotoxic stress

Next, we sought to determine how a deficiency in mitochondrial fusion could affect JNK activation. The basal level of p-JNK in control cells was very low and upon treatment with 500 μM H_2O_2, a dramatic increase of p-JNK was observed in the nucleus as well as in mitochondria (Figure 4A). Under these conditions, p-JNK partly colocalized with mitochondria; however, this was abolished by the loss of MFN (Figure 4B). It was previously shown that Sab/SH3BP5 (SH3-domain binding protein 5) anchored at the outer mitochondria membrane directly interacts with JNK and mediating JNK activation (51,52). To assess the relationship between mitochondrial fusion and mitochondrial JNK, we affinity-purified FLAG-tagged Sab expressed in U2OS cells. Co-IP revealed that Sab interacted with not only JNK, but also mitochondrial shaping proteins including MFN1, MFN2, and MFF; by contrast, we observed weak or no interactions with OPA1, hFis1, Tom20 and DRP1 (Figure 4C). This is the first indication of a functional link between Sab, JNK, and the mitochondrial fusion machinery. In cells overexpressing FLAG-Sab, we observed stable interactions between Sab and JNK regardless of the presence of H_2O_2 (Figure 4D). At the endogenous levels, JNK interacted with Sab in the cells exposed to Phleo and this interaction was considerably reduced in MFN1-depleted cells (Figure 4E). Similar results were obtained in cells exposed to high-glucose conditions: H_2O_2 induced an interaction of Sab with JNK and this interaction was attenuated in cells cultured in 50 mM of glucose for 5 h (Figure 4F). Given the important role of Sab in JNK activation, we investigated whether silencing of Sab protein mediates the DDR primarily through JNK activation. As shown in Figure 4G, depletion of Sab by siRNA lessened the p-JNK level, which caused a significant reduction in p-ATM and γ-H2AX levels (Figure 4G, H). Together, these results reveal a novel retrograde signaling pathway from mitochondria to the nucleus, showing that the interaction of Sab with the mitochondrial fusion machinery acts as an upstream modulator of JNK activation, which in turn primes ATM-dependent DDR signaling.

Mitochondrial fusion–dependent JNK signaling is crucial for efficient DNA repair

Because p-ATM and γH2AX are much reduced in cells deficient for mitochondrial fusion (Figure 3), we next examined the activities of downstream DDR signaling and DNA repair. Two mechanistically distinct pathways have evolved to eliminate DSBs from the genome: NHEJ and HR repair, both of which act to preserve genome integrity. Among the factors recruited to DSB sites, BRCA1 directs the repair pathways to HR, whereas 53BP1-RIF1 at unresected DNA ends drives NHEJ (11,12). We observed that the substantial accumulation of BRCA1 and 53BP1 foci in response to Phleo treatment was significantly reduced in cells defective in mitochondrial fusion (Figure 5A, B). Next, we examined repair of DSBs by HR and NHEJ using plasmid-based GFP-reporters that contain I-Sce1 endonuclease recognition sites. A set of reporters require either access to homology (DR-GFP) or end joining (EJ-GFP) between distal DSB ends of two tandem I-Sce1 site (39,40). ATM inhibitor significantly lowered the efficiency of HR repair and similarly, cells depleted of MFN1 showed a significant reduction in HR. Likewise, either Sab or JNK by siRNAs significantly reduced the HR efficiency (Figure 5C). Similarly, NHEJ was much reduced in cells silenced for MFN1, OPA1, Sab or JNK (Figure 5D) Consistent with this notion, inhibition of JNK activation by siRNA-mediated suppression of Sab and JNK significantly decreased NHEJ efficiency. Together, these results showed that mitochondrial fusion defects or inhibition of mitochondrial JNK activation substantially decrease both HR and NHEJ. Finally, we evaluated the repair efficiency of damaged chromatin using Comet assay; the tail image was automatically analyzed using the OpenComet software, which provides the tail moment profile. When U2OS cells were exposed to H_2O_2 for 30 min, both indexes were significantly increased and 4 h after wash-off (R4), suggesting that damaged chromatin was almost fully repaired (Figure 5E). By contrast, the damaged chromatin in cells with MFN1 shRNA was only slightly repaired, and most of them still retained the tail. Importantly, when we reintroduced FLAG-tagged MFN1 into MFN1-depleted cells, repair of the damaged chromatin was facilitated (Figure 5F). Together, our data collectively demonstrate that mitochondrial fusion–dependent JNK signaling is essential for proper DDR signaling and DNA repair. Our observations provide novel insight into the tight cooperation between DDR and mitochondrial fusion machinery along with cytosolic stress signals on the mitochondrial platform.

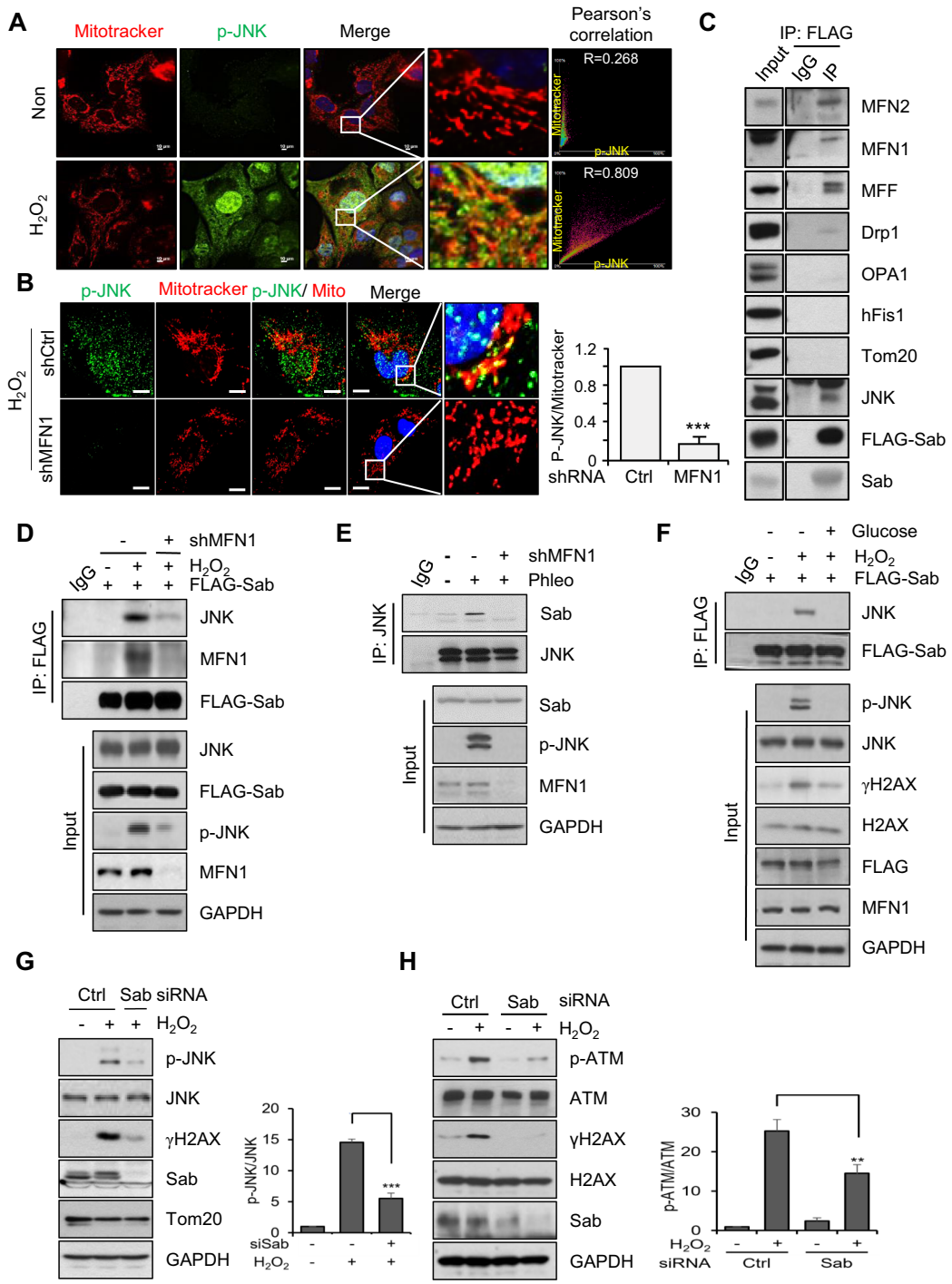

Figure 4. Sab-mitofusins interaction serves as a platform on which JNK is activated. (**A**) U2OS cells were immunostaind with anti-p-JNK (green) and MitoTracker (red) in the presence or absence of H_2O_2 (500 μM) for 20 min and imaged under Nikon A1 confocal microscopy. MitoTracker represents mitochondria, and Pearson's correlation between p-JNK and mitochondria markers was analyzed. scale bars, 10 μm. (**B**) U2OS cells stably expressing MFN1 shRNA were treated with H_2O_2 treatment for 20 min. U2OS cells were stained with anti-p-JNK (green), Mitotracker (red) and DAPI (blue). Bar graphs represent mean ± SEM from three independent experiments showing relative signal intensity of p-JNK (shCtrl $n = 36$ and shMFN1 $n = 42$) at the mitochondria. *** $P < 0.001$ versus control shRNA by two-sided unpaired Student's *t*-test. scale bars, 10 μm. (**C**) FLAG-Sab plasmid was transfected into U2OS cells and immunoprecipitated with anti-FLAG antibody, followed by immunoblotting with the indicated antibodies. (**D**) Control or MFN1 shRNA expressing U2OS cells were transfected with FLAG-Sab plasmid and treated with H_2O_2 for 20 min. Cell lysates were followed by immunoprecipitation using anti-FLAG and immunoblotted with the anti-JNK antibodies. (**E**) Control or MFN1 depleted U2OS cells were treated with Phleo for 2 h. Cell lysates were used for immunoprecipitation with anti-JNK antibody and followed by immunoblotting with anti-Sab antibodies. (**F**) U2OS were transfected with FLAG-Sab plasmid. Cells were subjected to H_2O_2 for 20 min in presence of 50 mM glucose for 5 h. Cell lysates were immunoprecipitated with FLAG antibody and immunoblotted with the anti-JNK antibodies. (**G, H**) U2OS cells were transfected with siRNA against Sab and obtained after H_2O_2 treatment for 20 min. The p-JNK or p-ATM expression levels were quantified by using imageJ. Bars represent mean ± SEM from three independent experiments. *** $P < 0.001$ versus control siRNA by two-sided unpaired Student's *t*-test.

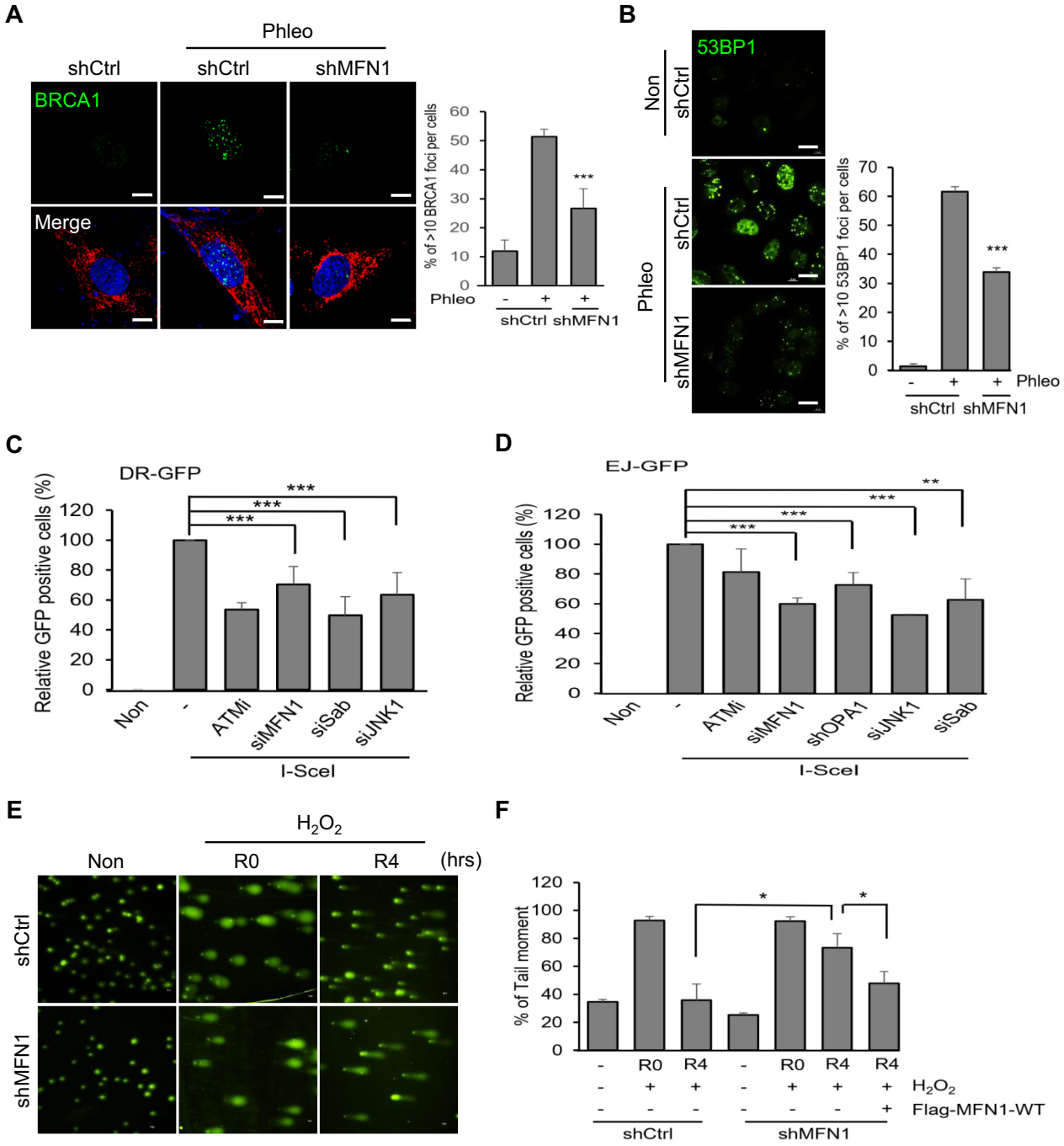

Figure 5. Mitochondrial morphodynamics affects DNA damage repair signaling. (**A**) MFN1-depleted cells were treated with Phleo for 2 h. U2OS cells were stained with anti-BRCA1 (green), Mitotracker (red) and DAPI (blue). Bar graph represents quantification of >10 foci of BRCA1. Cells were counted in three independent experiments (shCtrl $n = 245$ and shMFN1 $n = 312$). ***$P < 0.001$ vs control shRNA by two-sided unpaired Student's t-test. Scale bar, 10 μm. (**B**) MFN1-depleted U2OS cells were treated with Phleo for 2 h and immunostained with anti-53BP1 antibody. The percentage of >10 foci of 53BP1 per cell was shown in three dependent experiments (shCtrl n = 352 and shMFN1 $n = 279$). ***$P < 0.001$ vers control shRNA by two-sided unpaired Student's t-test. scale bars, 10 μm. (**C**) U2OS HR reporter cells were transfected with indicated siRNAs. After 24h, I-Sce1 nuclease-expressing vector was transfected into reporter cells. After 48 h, GFP-positive cells were calculated by FACS. An ATM inhibitor (ATMi) was used as a HR positive control. Bars represent mean ± SEM from three independent experiments. *** $P < 0.001$ versus control shRNA by two-sided unpaired Student's t-test. (**D**) U2OS NHEJ reporter cells were transfected with MFN1, Sab and JNK1 siRNA or shOPA1. Twenty-four hours after transfection, I-Sce1 nuclease-expressing vector was transfected into reporter cells. After 48 h, the number of FACS-sorted GFP-positive cells indicate repair efficiency and is normalized to mock control. An ATM inhibitor (ATMs) was used as an HR/ NHEJ positive control. Bars represent mean ± SEM from three independent experiments. **$P < 0.005$, *** $P < 0.001$ versus control shRNA by two-sided unpaired Student's t-test. (**E**) H_2O_2-induced DDR was examined by Alkaline comet assays. The control or MFN1-depleted U2OS cells were subjected to H_2O_2 (500 μM) treatment for 20 min. Cells were released with fresh medium for 4 h after exposure of DNA damage and proceeded to comet assay. scale bars, 10 μm. (**F**) Average tail moments of cells are shown in the comet assay. Bars represent mean ± SEM from three independent experiments. *$P < 0.05$ versus control shRNA by two-sided unpaired Student's t-test.

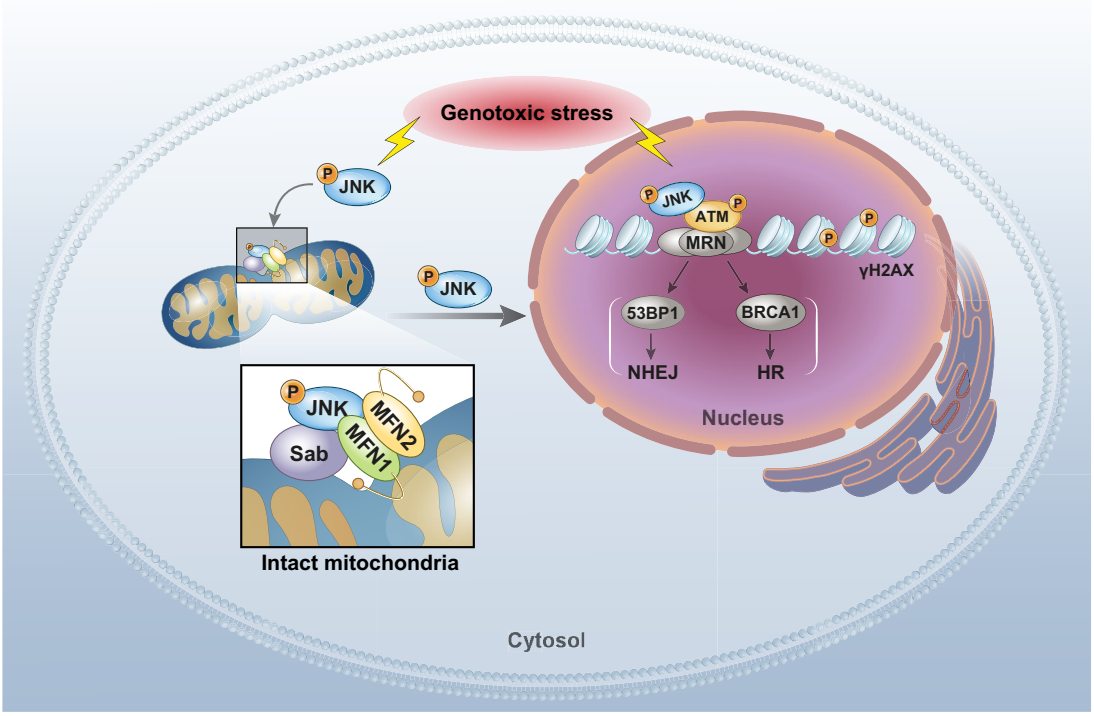

Figure 6. A proposed model for the cross-talk between nuclear DDR and mitochondrial morphofunctional pathway. In our model, ATM-mediated nuclear DDR relies on a mitochondrial morphofunctional pathway consisting of MFN1/MFN2, Sab (SH3BP5) and p-JNK.

DISCUSSION

In this study, we have revealed a key connection between nuclear DDR and the mitochondrial morphofunctional pathway. ATM-mediated nuclear DDR relies on a mitochondria-mediated signal consisting of MFN1/MFN2, Sab (SH3BP5), and JNK (Figure 6). These components work together as follows: (i) the mitochondria fusion machinery directly regulates JNK signaling; (ii) JNK activation is important for ATM-dependent DDR and repair, and (iii) cells efficiently integrate signals from various organelles (nucleus, cytosol and mitochondria) to respond to genotoxic stress. Thus, mitochondria indeed serve as a signaling hub for the regulation of cellular homeostasis and organismal functions beyond the regulation of bioenergetics and metabolism. Our observations provide novel insight into how cells efficiently integrate nuclear and cytosolic stress signals.

In cells, mitochondrial populations undergo continuous cycles of fission and fusion to maintain organelle integrity and cellular homeostasis; however, the equilibrium between fusion and fission can be disturbed by physiological cues as well as pathological conditions (18–20). Transient formation of hyperfused tubular mitochondria appears to ameliorate cellular stress. Indeed, elongated mitochondria are observed in cells exposed to starvation or hypoxia (19–22). Likewise, when U2OS cells were exposed to Phleo or H_2O_2, we observed transiently hyperfused mitochondria that returned to normal under fluorescence microscopy (Supplementary Figure S1A, B). In these conditions, mitochondria are capable of sensing stress and sending the morphofunctional signal to the nucleus. In fact, MFN1 KO or KD cells with impaired mitochondria fusion did not exhibit differences in mitochondrial membrane potential (MMP) or ROS levels after treatment with Phleo (Supplementary Figure S5). By contrast, when cells were continuously exposed to high glucose for 5 h, the mitochondria underwent fragmentation (Supplementary Figure S3A) and the cells did not properly respond to the genotoxic stress. The importance of mitochondria dynamics in DDR signaling cannot be overemphasized, as cells released from high-glucose stress recovered their γH2AX levels (Figure 1I). Thus, retention of the capacity to undergo mitochondrial fission and fusion determines the mitochondrial morphofunctional signal. However, it is worthwhile mentioning that prolonged exposure of cells to H_2O_2 can increase mitochondrial fragmentation (53). In addition, although ATM is the representative master kinase in the DDR, ATR and DNA-PKcs also reside at the apex of mammalian DDR and phosphorylate overlapping downstream substrates (54). As time passes different types of DNA damage occur, which can trigger the activation of ATR and DNA-PKcs.

JNK activation upon cellular stress plays a critical role in modulating cell death. Sustained JNK activation is linked to apoptotic DNA fragmentation (50,55) and the mitochondrial apoptotic pathways (56). The mitochondrial outer membrane protein, Sab (SH3BP5), provides a docking site for JNK. In a liver injury model, knock-down of Sab results in the inhibition of sustained JNK activation as well as JNK-mediated toxicity. Moreover, the JNK–Sab–ROS activation loop forms an intramitochondrial signal transduction pathway (57). Our findings here demonstrated that formation of the binding station between JNK, Sab, and MFN1/MFN2 protein are crucial for JNK activity and

ATM-mediated nuclear DNA damage signaling that contributes to the maintenance of genomic integrity. Thus, the Sab–JNK interaction is a double-edged sword, determining whether a cell undergoes programmed cell death or survives following DNA repair. In this regard, mitochondrial dynamics machinery may play a set-point role because Sab interacted with not only JNK, but also with MFN1 and MFN2 (Figure 4C). Moreover, we observed a functional link between Sab and JNK in cells defective in mitochondrial fusion. These findings provide critical insights linking the vital roles of mitochondrial dynamics to the JNK activation, and subsequently to the DNA damage response and repair signaling. On the other hand, sustained depletion of hFis1 by itself almost completely disrupts mitochondrial dynamics, leading to continuous mitochondrial elongation. Prolonged mitochondrial elongation induced by hFis1 depletion becomes cellular stress, triggering nuclear accumulation of γH2AX and cellular senescence (24). These were accompanied by a significant transcriptional reduction in cell cycle regulators (24,58). Likewise, another group also showed that replication-initiated DNA damage signaling was activated by DRP1 knockdown in an ATM- and ATR-dependent manner (59). An improved understanding of the modulation of DDR signaling mediated by mitochondria morphofunction may facilitate the development of new strategies with clinical implications for cancer patients who receive genotoxic anticancer drugs.

DATA AVAILABILITY

All data supporting the findings of this study are available within the article and its supplementary data.

SUPPLEMENTARY DATA

Supplementary Data are available at NAR Online.

ACKNOWLEDGEMENTS

DR-GFP or EJ-GFP containing stable cell lines and the I-Sce1 constructs were kindly provided by Dr Jeremy Stark (City of Hope National Medical Center). In addition, U2OS-2-6-5 cells were provided by Dr Green Rosenberg (University of Pennsylvania) with kind generosity.
Author contributions: N.T.K.O., H.-S.L. designed experiments, analyzed the results; H.-S.L., N.T.K.O. performed immunocytochemistry, live-cell imaging and cell survival assay; Y.-J.P., J.H., Y.H.K. prepared for plasmid construction, immunoprecipitation, and Fok1 immunocytochemistry; N.T.K.O., H.-S.L., W.-C.L. analyzed the results and commented on the manuscript; W.-C.L. and H.C. wrote the manuscript.

FUNDING

National Research Foundation of Korea grants funded by the Korean government (MSIP) [NRF-2020R1I1A1A01074047, NRF-2020R1A2C3011423, NRF-2020R1A2C4002527, NRF-2019S1A5A2A03051702]. Funding for open access charge: National Research Foundation of Korea [NRF-2020R1A2C3011423].

Conflict of interest statement. None declared.

REFERENCES

1. Lukas,J., Lukas,C. and Bartek,J. (2011) More than just a focus: the chromatin response to DNA damage and its role in genome integrity maintenance. *Nat. Cell Biol.*, **13**, 1161–1169.
2. Aymard,F., Aguirrebengoa,M., Guillou,E., Javierre,B.M., Bugler,B., Arnould,C., Rocher,V., Iacovoni,J.S., Biernacka,A., Skrzypczak,M. *et al.* (2017) Genome-wide mapping of long-range contacts unveils clustering of DNA double-strand breaks at damaged active genes. *Nat. Struct. Mol. Biol.*, **24**, 353–361.
3. Lee,J.H. and Paull,T.T. (2005) ATM activation by DNA double-strand breaks through the Mre11-Rad50-Nbs1 complex. *Science*, **308**, 551–554.
4. van den Bosch,M., Bree,R.T. and Lowndes,N.F. (2003) The MRN complex: coordinating and mediating the response to broken chromosomes. *EMBO Rep.*, **4**, 844–849.
5. Iacovoni,J.S., Caron,P., Lassadi,I., Nicolas,E., Massip,L., Trouche,D. and Legube,G. (2010) High-resolution profiling of gammaH2AX around DNA double strand breaks in the mammalian genome. *EMBO J.*, **29**, 1446–1457.
6. Uckelmann,M. and Sixma,T.K. (2017) Histone ubiquitination in the DNA damage response. *DNA Repair (Amst.)*, **56**, 92–101.
7. Rossetto,D., Truman,A.W., Kron,S.J. and Cote,J. (2010) Epigenetic modifications in double-strand break DNA damage signaling and repair. *Clin. Cancer Res.*, **16**, 4543–4552.
8. Escribano-Diaz,C., Orthwein,A., Fradet-Turcotte,A., Xing,M., Young,J.T., Tkac,J., Cook,M.A., Rosebrock,A.P., Munro,M., Canny,M.D. *et al.* (2013) A cell cycle-dependent regulatory circuit composed of 53BP1-RIF1 and BRCA1-CtIP controls DNA repair pathway choice. *Mol. Cell*, **49**, 872–883.
9. Mirman,Z., Lottersberger,F., Takai,H., Kibe,T., Gong,Y., Takai,K., Bianchi,A., Zimmermann,M., Durocher,D. and de Lange,T. (2018) 53BP1-RIF1-shieldin counteracts DSB resection through CST- and Polalpha-dependent fill-in. *Nature*, **560**, 112–116.
10. Jackson,S.P. and Bartek,J. (2009) The DNA-damage response in human biology and disease. *Nature*, **461**, 1071–1078.
11. Daugaard,M., Baude,A., Fugger,K., Povlsen,L.K., Beck,H., Sorensen,C.S., Petersen,N.H., Sorensen,P.H., Lukas,C., Bartek,J. *et al.* (2012) LEDGF (p75) promotes DNA-end resection and homologous recombination. *Nat. Struct. Mol. Biol.*, **19**, 803–810.
12. Chang,H.H.Y., Pannunzio,N.R., Adachi,N. and Lieber,M.R. (2017) Non-homologous DNA end joining and alternative pathways to double-strand break repair. *Nat. Rev. Mol. Cell Biol.*, **18**, 495–506.
13. Smirnova,E., Griparic,L., Shurland,D.L. and van der Bliek,A.M. (2001) Dynamin-related protein Drp1 is required for mitochondrial division in mammalian cells. *Mol. Biol. Cell*, **12**, 2245–2256.
14. Palmer,C.S., Osellame,L.D., Laine,D., Koutsopoulos,O.S., Frazier,A.E. and Ryan,M.T. (2011) MiD49 and Mid51, new components of the mitochondrial fission machinery. *EMBO Rep.*, **12**, 565–573.
15. Zhao,J., Liu,T., Jin,S., Wang,X., Qu,M., Uhlen,P., Tomilin,N., Shupliakov,O., Lendahl,U. and Nister,M. (2011) Human MIEF1 recruits Drp1 to mitochondrial outer membranes and promotes mitochondrial fusion rather than fission. *EMBO J.*, **30**, 2762–2778.
16. Loson,O.C., Song,Z., Chen,H. and Chan,D.C. (2013) Fis1, Mff, Mid49, and Mid51 mediate Drp1 recruitment in mitochondrial fission. *Mol. Biol. Cell*, **24**, 659–667.
17. Koshiba,T., Detmer,S.A., Kaiser,J.T., Chen,H., McCaffery,J.M. and Chan,D.C. (2004) Structural basis of mitochondrial tethering by mitofusin complexes. *Science*, **305**, 858–862.
18. Chen,H. and Chan,D.C. (2010) Physiological functions of mitochondrial fusion. *Ann. N. Y. Acad. Sci.*, **1201**, 21–25.
19. Rambold,A.S., Kostelecky,B., Elia,N. and Lippincott-Schwartz,J. (2011) Tubular network formation protects mitochondria from autophagosomal degradation during nutrient starvation. *Proc. Natl. Acad. Sci. U.S.A.*, **108**, 10190–10195.
20. Shutt,T.E. and McBride,H.M. (2013) Staying cool in difficult times: mitochondrial dynamics, quality control and the stress response. *Biochim. Biophys. Acta*, **1833**, 417–424.
21. Tondera,D., Grandemange,S., Jourdain,A., Karbowski,M., Mattenberger,Y., Herzig,S., Da Cruz,S., Clerc,P., Raschke,I.,

Merkwirth,C. *et al.* (2009) SLP-2 is required for stress-induced mitochondrial hyperfusion. *EMBO J.*, **28**, 1589–1600.
22. Park,Y.Y., Nguyen,O.T., Kang,H. and Cho,H. (2014) MARCH5-mediated quality control on acetylated Mfn1 facilitates mitochondrial homeostasis and cell survival. *Cell Death Dis.*, **5**, e1172.
23. Zemirli,N., Pourcelot,M., Ambroise,G., Hatchi,E., Vazquez,A. and Arnoult,D. (2014) Mitochondrial hyperfusion promotes NF-kappaB activation via the mitochondrial E3 ligase MULAN. *FEBS J.*, **281**, 3095–3112.
24. Lee,S., Jeong,S.Y., Lim,W.C., Kim,S., Park,Y.Y., Sun,X., Youle,R.J. and Cho,H. (2007) Mitochondrial fission and fusion mediators, hFis1 and OPA1, modulate cellular senescence. *J. Biol. Chem.*, **282**, 22977–22983.
25. Park,Y.Y., Lee,S., Karbowski,M., Neutzner,A., Youle,R.J. and Cho,H. (2010) Loss of MARCH5 mitochondrial E3 ubiquitin ligase induces cellular senescence through dynamin-related protein 1 and mitofusin 1. *J. Cell Sci.*, **123**, 619–626.
26. Yu,T., Robotham,J.L. and Yoon,Y. (2006) Increased production of reactive oxygen species in hyperglycemic conditions requires dynamic change of mitochondrial morphology. *Proc. Natl. Acad. Sci. U.S.A.*, **103**, 2653–2658.
27. McKenzie,M.D., Jamieson,E., Jansen,E.S., Scott,C.L., Huang,D.C., Bouillet,P., Allison,J., Kay,T.W., Strasser,A. and Thomas,H.E. (2010) Glucose induces pancreatic islet cell apoptosis that requires the BH3-only proteins Bim and Puma and multi-BH domain protein Bax. *Diabetes*, **59**, 644–652.
28. Karbowski,M., Lee,Y.J., Gaume,B., Jeong,S.Y., Frank,S., Nechushtan,A., Santel,A., Fuller,M., Smith,C.L. and Youle,R.J. (2002) Spatial and temporal association of Bax with mitochondrial fission sites, Drp1, and Mfn2 during apoptosis. *J. Cell Biol.*, **159**, 931–938.
29. Wu,Q.R., Zheng,D.L., Liu,P.M., Yang,H., Li,L.A., Kuang,S.J., Lai,Y.Y., Rao,F., Xue,Y.M., Lin,J.J. *et al.* (2021) High glucose induces Drp1-Mediated mitochondrial fission via the Orai1 calcium channel to participate in diabetic cardiomyocyte hypertrophy. *Cell Death. Dis.*, **12**, 216.
30. Youle,R.J. and Narendra,D.P. (2011) Mechanisms of mitophagy. *Nat. Rev. Mol. Cell Biol.*, **12**, 9–14.
31. Scheibye-Knudsen,M., Fang,E.F., Croteau,D.L., Wilson,D.M. 3rd and Bohr,V.A. (2015) Protecting the mitochondrial powerhouse. *Trends Cell Biol.*, **25**, 158–170.
32. Moretton,A., Morel,F., Macao,B., Lachaume,P., Ishak,L., Lefebvre,M., Garreau-Balandier,I., Vernet,P., Falkenberg,M. and Farge,G. (2017) Selective mitochondrial DNA degradation following double-strand breaks. *PLoS One*, **12**, e0176795.
33. Peeva,V., Blei,D., Trombly,G., Corsi,S., Szukszto,M.J., Rebelo-Guiomar,P., Gammage,P.A., Kudin,A.P., Becker,C., Altmuller,J. *et al.* (2018) Linear mitochondrial DNA is rapidly degraded by components of the replication machinery. *Nat. Commun.*, **9**, 1727.
34. West,A.P., Khoury-Hanold,W., Staron,M., Tal,M.C., Pineda,C.M., Lang,S.M., Bestwick,M., Duguay,B.A., Raimundo,N., MacDuff,D.A. *et al.* (2015) Mitochondrial DNA stress primes the antiviral innate immune response. *Nature*, **520**, 553–557.
35. Sandy,Z., da Costa,I.C. and Schmidt,C.K. (2020) More than meets the ISG15: emerging roles in the DNA damage response and beyond. *Biomolecules*, **10**, 1557.
36. Azarm,K. and Smith,S. (2020) Nuclear PARPs and genome integrity. *Genes Dev.*, **34**, 285–301.
37. Wu,Z., Oeck,S., West,A.P., Mangalhara,K.C., Sainz,A.G., Newman,L.E., Zhang,X.O., Wu,L., Yan,Q., Bosenberg,M. *et al.* (2019) Mitochondrial DNA stress signalling protects the nuclear genome. *Nat Metab*, **1**, 1209–1218.
38. Tigano,M., Vargas,D.C., Tremblay-Belzile,S., Fu,Y. and Sfeir,A. (2021) Nuclear sensing of breaks in mitochondrial DNA enhances immune surveillance. *Nature*, **591**, 477–481.
39. Gunn,A. and Stark,J.M. (2012) I-SceI-based assays to examine distinct repair outcomes of mammalian chromosomal double strand breaks. *Methods Mol. Biol.*, **920**, 379–391.
40. Liu,S., Fan,Z., Geng,Z., Zhang,H., Ye,Q., Jiao,S. and Xu,X. (2013) PIAS3 promotes homology-directed repair and distal non-homologous end joining. *Oncol. Lett.*, **6**, 1045–1048.
41. Rehman,J., Zhang,H.J., Toth,P.T., Zhang,Y., Marsboom,G., Hong,Z., Salgia,R., Husain,A.N., Wietholt,C. and Archer,S.L. (2012) Inhibition of mitochondrial fission prevents cell cycle progression in lung cancer. *FASEB J.*, **26**, 2175–2186.
42. Zhang,Y., Lee,J.H., Paull,T.T., Gehrke,S., D'Alessandro,A., Dou,Q., Gladyshev,V.N., Schroeder,E.A., Steyl,S.K., Christian,B.E. *et al.* (2018) Mitochondrial redox sensing by the kinase ATM maintains cellular antioxidant capacity. *Sci. Signal*, **11**, 538.
43. Yu,R., Jin,S.B., Lendahl,U., Nister,M. and Zhao,J. (2019) Human Fis1 regulates mitochondrial dynamics through inhibition of the fusion machinery. *EMBO J.*, **38**, e99748.
44. Kobayashi,S., Zhao,F., Zhang,Z., Kobayashi,T., Huang,Y., Shi,B., Wu,W. and Liang,Q. (2020) Mitochondrial fission and mitophagy coordinately restrict high glucose toxicity in cardiomyocytes. *Front. Physiol.*, **11**, 604069.
45. Montaigne,D., Marechal,X., Coisne,A., Debry,N., Modine,T., Fayad,G., Potelle,C., El Arid,J.M., Mouton,S., Sebti,Y. *et al.* (2014) Myocardial contractile dysfunction is associated with impaired mitochondrial function and dynamics in type 2 diabetic but not in obese patients. *Circulation*, **130**, 554–564.
46. Johnson,G.L. and Lapadat,R. (2002) Mitogen-activated protein kinase pathways mediated by ERK, JNK, and p38 protein kinases. *Science*, **298**, 1911–1912.
47. Hotamisligil,G.S. and Davis,R.J. (2016) Cell signaling and stress responses. *Cold Spring Harb. Perspect. Biol.*, **8**, a006072.
48. Johnson,G.L. and Nakamura,K. (2007) The c-jun kinase/stress-activated pathway: regulation, function and role in human disease. *Biochim. Biophys. Acta*, **1773**, 1341–1348.
49. Aymard,F., Bugler,B., Schmidt,C.K., Guillou,E., Caron,P., Briois,S., Iacovoni,J.S., Daburon,V., Miller,K.M., Jackson,S.P. *et al.* (2014) Transcriptionally active chromatin recruits homologous recombination at DNA double-strand breaks. *Nat. Struct. Mol. Biol.*, **21**, 366–374.
50. Lu,C., Zhu,F., Cho,Y.Y., Tang,F., Zykova,T., Ma,W.Y., Bode,A.M. and Dong,Z. (2006) Cell apoptosis: requirement of H2AX in DNA ladder formation, but not for the activation of caspase-3. *Mol. Cell*, **23**, 121–132.
51. Wiltshire,C., Matsushita,M., Tsukada,S., Gillespie,D.A. and May,G.H. (2002) A new c-Jun N-terminal kinase (JNK)-interacting protein, Sab (SH3BP5), associates with mitochondria. *Biochem. J.*, **367**, 577–585.
52. Chambers,J.W., Cherry,L., Laughlin,J.D., Figuera-Losada,M. and Lograsso,P.V. (2011) Selective inhibition of mitochondrial JNK signaling achieved using peptide mimicry of the Sab kinase interacting motif-1 (KIM1). *ACS Chem. Biol.*, **6**, 808–818.
53. Fan,X., Hussien,R. and Brooks,G.A. (2010) H2O2-induced mitochondrial fragmentation in C2C12 myocytes. *Free Radic. Biol. Med.*, **49**, 1646–1654.
54. Menolfi,D. and Zha,S. (2020) ATM, ATR and DNA-PKcs kinases-the lessons from the mouse models: inhibition not equal deletion. *Cell Biosci.*, **10**, 8.
55. Sluss,H.K. and Davis,R.J. (2006) H2AX is a target of the JNK signaling pathway that is required for apoptotic DNA fragmentation. *Mol. Cell*, **23**, 152–153.
56. Tsuruta,F., Sunayama,J., Mori,Y., Hattori,S., Shimizu,S., Tsujimoto,Y., Yoshioka,K., Masuyama,N. and Gotoh,Y. (2004) JNK promotes Bax translocation to mitochondria through phosphorylation of 14-3-3 proteins. *EMBO J.*, **23**, 1889–1899.
57. Hirata,Y., Inoue,A., Suzuki,S., Takahashi,M., Matsui,R., Kono,N., Noguchi,T. and Matsuzawa,A. (2020) trans-Fatty acids facilitate DNA damage-induced apoptosis through the mitochondrial JNK-Sab-ROS positive feedback loop. *Sci. Rep.*, **10**, 2743.
58. Lee,S., Park,Y.Y., Kim,S.H., Nguyen,O.T., Yoo,Y.S., Chan,G.K., Sun,X. and Cho,H. (2014) Human mitochondrial Fis1 links to cell cycle regulators at G2/M transition. *Cell. Mol. Life Sci.*, **71**, 711–725.
59. Qian,W., Choi,S., Gibson,G.A., Watkins,S.C., Bakkenist,C.J. and Van Houten,B. (2012) Mitochondrial hyperfusion induced by loss of the fission protein Drp1 causes ATM-dependent G2/M arrest and aneuploidy through DNA replication stress. *J. Cell Sci.*, **125**, 5745–5757.